

# Unruh-deWitt detectors in quantum superpositions of trajectories

Joshua Foo,<sup>1,\*</sup> Sho Onoe,<sup>1</sup> and Magdalena Zych<sup>2,†</sup>

<sup>1</sup>*Centre for Quantum Computation and Communication Technology, School of Mathematics and Physics,  
The University of Queensland, St. Lucia, Queensland, 4072, Australia*

<sup>2</sup>*Centre for Engineered Quantum Systems, School of Mathematics and Physics,  
The University of Queensland, St. Lucia, Queensland, 4072, Australia*

(Dated: October 5, 2020)

Unruh-deWitt detectors have been utilised widely as probes for quantum particles, entanglement and space-time curvature. Here, we extend the standard treatment of an Unruh-deWitt detector interacting with a massless, scalar field to include the detector travelling in a quantum superposition of classical trajectories. We derive perturbative expressions for the final state of the detector, and show that it depends on field correlation functions evaluated locally along the individual trajectories, as well as non-locally between the superposed trajectories. By applying our general approach to a detector travelling in a superposition of two uniformly accelerated trajectories, including those with equal and differing proper accelerations, we discover novel interference effects in the emission and absorption spectra. These effects can be traced to causal relations between the superposed trajectories. Finally, we show that in general, such a detector does not thermalise even if the superposed paths would individually yield the same thermal state.

## I. INTRODUCTION

The Unruh-deWitt (UdW) detector is widely used as a probe of the foundational aspects of relativistic quantum fields and the structure of spacetime. The standard formulation of the model describes an idealised particle detector – typically, a point-like two-level system – that follows a classical worldline and whose internal states couple to the field [1]. For example, consider the detector interacting with the massless scalar field in the Minkowski vacuum, and traversing a uniformly accelerated trajectory in spacetime with proper acceleration  $\kappa$ . Unlike an inertial detector, which register no particles, the accelerated detector perceives a thermalised quantum state, radiating particles at the Unruh temperature,

$$T_U = \frac{\kappa}{2\pi}. \quad (1)$$

This phenomenon is a manifestation of the Unruh effect, a prediction of relativistic quantum field theory that asserts that the experience of observers – i.e. detectors – interacting with quantum fields is frame-dependent [2]. The utility and simplicity of the UdW detector model has facilitated its application to numerous related problems. Perturbative [3–5] and non-perturbative [6–8] approaches have been used to study entanglement dynamics and detection in settings such as non-inertial reference frames and expanding universes [9–14], and detector responses in curved spacetimes [15–19] and higher-dimensional topologies [20, 21]. A list of further results can be found in [22].

While the UdW detector model has been devised as a probe for quantum particles, the quantum effects associated with its motion are just beginning to be explored. In particular, [23] studies the absorption and emission of a UdW detector with a position degree of freedom described by a freely expanding

wavefunction. In this work, we develop a general description of a single UdW detector coupling to a massless, scalar field and travelling in a *quantum superposition of classical trajectories*. More specifically, we are interested in the response of such a detector when subjected to a combination of relativistic and quantum-mechanical effects. By initialising the detector in a quantum-controlled superposition of uniformly accelerated trajectories (parallel and anti-parallel accelerations, and trajectories sharing a Rindler horizon with differing proper accelerations), we discover the presence of novel interference dynamics in the emission and absorption spectra. These effects depend on the causal relations between the trajectories of the superposition, mediated by the non-local correlation functions evaluated along different trajectories.

Such a model may engender new approaches for studying fundamental aspects of relativistic quantum field theory. For example, it provides an operational approach for studying the behaviour of quantum fields in *quantum reference frames* (reference frames defined with respect to systems possessing quantum indeterminacy) [24], since the detector either does not have a well-defined spacetime location (parallel, anti-parallel accelerations) or proper acceleration (differing accelerations). In the latter case, one may ask whether the notion of a coherent superposition of temperatures can be meaningfully defined, given that the individual accelerations are associated with a unique Unruh temperature. Furthermore, the possibility of superposing the temporal order of the detector’s interaction with the field may enable it to probe the causal structure of spacetime [25–27]. We comment on the former question in Sec. III while we propose the latter as a future direction in Sec. V. As we elaborate upon in Sec. V, quantum-controlled UdW detectors also unveil a deeper connection between coherently controlled quantum channels [28–31], relativistic quantum information [32], and quantum thermodynamics [33].

This paper is organised as follows: in Sec. II, we review the UdW detector model coupling to a massless, scalar field, and apply it to a detector in an arbitrary superposition of relativistic – i.e. classical – trajectories. We then derive expressions for the conditional transition probability and instantaneous

\* [joshua.foo@uqconnect.edu.au](mailto:joshua.foo@uqconnect.edu.au)

† [m.zych@uq.edu.au](mailto:m.zych@uq.edu.au)

transition rate of the detector to second-order in perturbation theory. In Sec. III, we apply our formalism to a two-trajectory superposition of uniformly accelerated paths in parallel and anti-parallel motion, and those sharing a Rindler horizon but with differing proper accelerations. We conclude with some final remarks and directions for future research. Throughout, we use natural units  $c = \hbar = k_B = 1$  and the metric signature  $(-, +, +, +)$ .

## II. FINAL DETECTOR STATE, TRANSITION PROBABILITIES AND RATES

### A. Unruh-deWitt Model

We begin by considering a two-level Unruh-deWitt detector initially in its ground state  $|g\rangle$  and coupled to the real, massless scalar field,  $\hat{\Phi}(x(\tau))$ , in (1+3)-dimensional Minkowski spacetime. Suppose that the field is also in its ground state, the Minkowski vacuum  $|0_M\rangle$ . To initialise the detector in a trajectory superposition, we introduce a control degree of freedom,  $c_i$ , whose states  $|c_i\rangle$  designate the individual paths which the detector takes. The state of the system can be expressed as

$$|\Psi\rangle_S = |c\rangle \otimes |0_M\rangle \otimes |g\rangle \quad \text{where} \quad |c\rangle = \frac{1}{\sqrt{N}} \sum_{i=1}^N |c_i\rangle. \quad (2)$$

where  $|c_i\rangle$  are orthogonal states. Furthermore, we neglect any free dynamics of the control and assume that it is unaffected by measurements of the internal states of the detector such as its energy levels.

Now, the coupling of the detector to the field is described by the interaction Hamiltonian,

$$\hat{H}_I(\tau) = \sum_{i=1}^N \hat{\mathcal{H}}_i \otimes |c_i\rangle\langle c_i| \quad (3)$$

where

$$\hat{\mathcal{H}}_i(\tau) = \lambda \eta(\tau) \sigma(\tau) \hat{\Phi}(x_i(\tau)) \quad (4)$$

and  $\lambda \ll 1$  is a weak coupling constant,  $\eta(\tau)$  is a time-dependent switching function that governs the interaction,  $\sigma(\tau) = \sigma^+ e^{i\Omega\tau} + \text{h.c}$  is the interaction picture Pauli operator (with  $\sigma^+ = |e\rangle\langle g|$ ) for the detector with energy gap  $\Omega$  between the energy eigenstates  $|g\rangle, |e\rangle$ , and  $x_i(\tau)$  is the worldline of the  $i$ th path of the superposition. The evolution of the initial system state from an initial time  $\tau_0$  to final time  $\tau$  can be obtained by perturbatively expanding the time evolution operator using

the Dyson series,

$$\hat{U} = \sum_{i=1}^N |c_i\rangle\langle c_i| - i\lambda \underbrace{\int_{\tau_0}^{\tau} d\tau' \hat{H}_I(\tau')}_{\hat{U}^{(1)}} - \lambda^2 \underbrace{\int_{\tau_0}^{\tau} d\tau' \int_{\tau_0}^{\tau'} d\tau'' \hat{H}_I(\tau') \hat{H}_I(\tau'')}_{\hat{U}^{(2)}} + \mathcal{O}(\lambda^3) \quad (5)$$

where we have truncated the series beyond  $\mathcal{O}(\lambda^2)$ . The upper integration limit  $\tau'$  of  $\hat{U}^{(2)}$  enforces time-ordering of the Hamiltonians.  $\hat{U}$  can be expressed as

$$\hat{U} = \sum_{i=1}^N \hat{U}_i \otimes |c_i\rangle\langle c_i|, \quad (6)$$

where

$$\hat{U}_i = 1 - i\lambda \int_{\tau_0}^{\tau} d\tau' \hat{\mathcal{H}}_i(\tau') - \lambda^2 \int_{\tau_0}^{\tau} d\tau' \int_{\tau_0}^{\tau'} d\tau'' \hat{\mathcal{H}}_i(\tau') \hat{\mathcal{H}}_i(\tau'') + \mathcal{O}(\lambda^3) \quad (7)$$

are the contributions to  $\hat{U}$  along the  $i$ th trajectory of the superposition. The time evolution of  $|\Psi\rangle_S$  is thus given by

$$\hat{U}|\Psi\rangle_S = \frac{1}{\sqrt{N}} \sum_{i=1}^N \hat{U}_i \otimes |c_i\rangle|0_M\rangle|g\rangle \quad (8)$$

where the detector traversing the  $i$ th trajectory only interacts locally with the field  $\hat{\Phi}(x_i(\tau))$  along the worldline  $x_i(\tau)$ .

### B. Conditional Transition Probability

We consider the conditional transition probability and instantaneous transition rate of the detector given that the control is measured in a superposition state, which for simplicity we take to be  $|c\rangle$ . A generalised case, wherein the final state of the control is an arbitrary superposition, is discussed in Sec. IV. The final state of the detector-field system is given by  $\langle c|\hat{U}|\Psi\rangle_S = |\Psi\rangle_{FD}$

$$|\Psi\rangle_{FD} = \frac{1}{N} \sum_{i=1}^N \hat{U}_i |0_M\rangle|g\rangle. \quad (9)$$

The density matrix is

$$\hat{\rho}_{FD} = \frac{1}{N^2} \sum_{i,j=1}^N \underbrace{\hat{U}_i |0_M\rangle|g\rangle\langle g|0_M|\hat{U}_j^\dagger}_{\hat{\rho}_{ij,FD}} \quad (10)$$

Using the series expansion Eq. (5) and tracing over the final states of the field, the terms in the density matrix can be written as

$$\begin{aligned}
\hat{\rho}_{ij,D} = & |g\rangle\langle g| + \lambda^2|e\rangle\langle e| \int_{-\infty}^{\infty} d\tau' \chi(\tau') \int_{-\infty}^{\infty} d\tau'' \bar{\chi}(\tau'') \langle 0_M | \hat{\Phi}(x_j(\tau')) \hat{\Phi}(x_i(\tau'')) | 0_M \rangle \\
& - \lambda^2 |g\rangle\langle g| \int_{-\infty}^{\infty} d\tau' \chi(\tau') \int_{-\infty}^{\tau'} d\tau'' \bar{\chi}(\tau'') \langle 0_M | \hat{\Phi}(x_i(\tau')) \hat{\Phi}(x_i(\tau'')) | 0_M \rangle \\
& - \lambda^2 |g\rangle\langle g| \int_{-\infty}^{\infty} d\tau' \chi(\tau') \int_{-\infty}^{\tau'} d\tau'' \bar{\chi}(\tau'') \langle 0_M | \hat{\Phi}(x_j(\tau')) \hat{\Phi}(x_j(\tau'')) | 0_M \rangle
\end{aligned} \tag{11}$$

where  $\mathcal{W}^{ji} = \langle 0_M | \hat{\Phi}(x_i(\tau')) \hat{\Phi}(x_j(\tau'')) | 0_M \rangle$  are Wightman functions evaluated with respect to the trajectories  $x_i(\tau'), x_j(\tau'')$  [19] and we have defined  $\chi(\tau) = \eta(\tau)e^{-i\Omega\tau}$ . We have also taken  $\tau_0 \rightarrow -\infty$  and  $\tau \rightarrow \infty$  for illustration. Summing Eq. (10) over  $i, j$  yields the final state of the detector,

$$\hat{\rho}_D = \frac{1}{\mathcal{N}} \begin{bmatrix} 1 - \mathcal{P}_G & 0 \\ 0 & \mathcal{P}_E \end{bmatrix} \simeq \begin{bmatrix} 1 - \mathcal{P}_E & 0 \\ 0 & \mathcal{P}_E \end{bmatrix} + \mathcal{O}(\lambda^4) \tag{12}$$

where  $\mathcal{N} = (1 - \mathcal{P}_G + \mathcal{P}_E)^{-1}$  normalises the final state, conditioned upon measuring  $|c\rangle$ , and

$$\mathcal{P}_G = \frac{2\lambda^2}{N^2} \sum_{i=1}^N \int_{-\infty}^{\infty} d\tau' \chi(\tau') \int_{-\infty}^{\tau'} d\tau'' \bar{\chi}(\tau'') \mathcal{W}^{ii}(\tau', \tau'') \tag{13}$$

$$\mathcal{P}_E = \frac{\lambda^2}{N^2} \sum_{i,j=1}^N \int_{-\infty}^{\infty} d\tau' \chi(\tau') \int_{-\infty}^{\infty} d\tau'' \bar{\chi}(\tau'') \mathcal{W}^{ji}(\tau', \tau''). \tag{14}$$

This is our first new result. In the weak coupling limit ( $\lambda \ll 1$ ),  $\mathcal{P}_E$  is the conditional excitation probability of the detector, and contains products of first-order terms in the perturbative expansion. The new feature of this result is that  $\mathcal{P}_E$  contains two-point correlation functions – Wightman functions – evaluated *locally* along the individual trajectories ( $i = j$  and henceforth, *local* terms), as well as *non-locally* between any given pair of trajectories ( $i \neq j$  and henceforth, *non-local* or *interference* terms). Similar non-local correlation functions appear in the formulas used in two-detector entanglement harvesting scenarios. However in those settings, the integration over the non-local Wightman functions is time-ordered and differs by a phase factor to Eq. (14). Hence, they are interpreted as the amplitude for virtual particle exchange between *two detectors* on different worldlines, interacting locally with the field [10–13].

In Sec. III, we obtain semi-analytic results for the conditional excitation probability of a two-trajectory superposition in the simple case of a Gaussian switching function. Before presenting these results, we briefly review the key properties of the Wightman functions, and then derive expressions for the instantaneous transition rate.

### C. Wightman Functions

The behaviour of the Wightman functions  $\mathcal{W}^{ij}(\tau', \tau'')$  has been discussed widely in the literature [4, 5, 19, 34]. It was

shown by Schlicht that the typical  $i\epsilon$ -regularisation of the mode sum expansion of the fields, given by [19]

$$\mathcal{W}^{ij}(\tau', \tau'') = \lim_{\epsilon \rightarrow 0} \frac{-1/4\pi^2}{(t'_i - t''_j - i\epsilon)^2 - |\mathbf{x}'_i - \mathbf{x}''_j|^2} \tag{15}$$

can lead to Lorentz non-invariant transition rates when the switching functions possess sharp cut-offs [4]. Schlicht's solution was to spatially smear the field operator with a Lorentzian function – which models a point-like detector in the limit  $\epsilon \rightarrow 0$  after integration over  $(\tau', \tau'')$  – yielding the regularised result,

$$\mathcal{W}^{ij}(\tau', \tau'') = \frac{1/4\pi^2}{(\mathbf{x}'_i - \mathbf{x}''_j - i\epsilon(\dot{\mathbf{x}}'_i + \dot{\mathbf{x}}''_j))^2}. \tag{16}$$

where  $\dot{\mathbf{x}}'_i$  is the 4-velocity of the detector evaluated at  $\tau'$  along the  $i$ th trajectory of the superposition. In Sec. III, we utilise the Lorentzian-smeared regularisation, Eq. (16), to derive the conditional excitation probabilities and instantaneous transition rates of a detector travelling in a two-trajectory superposition. While *regulator-free* expressions for the instantaneous transition rate have been derived previously [5, 34], for the present work, Eq. (16) is convenient for obtaining numerical results.

### D. Instantaneous Transition Rates

The time-dependent behaviour of the detector will be non-trivially affected by field correlations between different trajectories in the superposition. This motivates us to study the instantaneous transition rate of the detector while the interaction is still on. Rather than taking the  $\tau \rightarrow \infty$  limit in Eq. (11), which models the measurement as occurring in the asymptotic future, we consider the evolution of the system *up to the time*  $\tau$ , so that the transition probability from Eq. (14) takes the form,

$$\mathcal{P}_E \propto \sum_{i,j=1}^N \int_{-\infty}^{\tau} d\tau' \chi(\tau') \int_{-\infty}^{\tau} d\tau'' \bar{\chi}(\tau'') \mathcal{W}^{ji}(\tau', \tau''), \tag{17}$$

where we have omitted the pre-factor ( $\lambda^2/N^2$ ) for brevity. This amounts to a cut-off in the switching function at the proper time  $\tau$ , which can be understood as a strong detector-observer interaction. Differentiating Eq. (17) with respect to  $\tau$ , using the identity  $\mathcal{W}^{ji}(\tau', \tau'') = \bar{\mathcal{W}}^{ij}(\tau'', \tau')$  and making a

change of variables  $s = \tau' - \tau''$  yields the following expression,

$$\dot{\mathcal{P}}_E \propto 2\eta(\tau)\text{Re} \sum_{i,j=1}^N \int_0^\infty ds e^{-i\Omega s} \eta(\tau-s) \mathcal{W}^{ji}(\tau, \tau-s), \quad (18)$$

where the limit  $\epsilon \rightarrow 0$  of the Wightman functions is taken after the integration and we have denoted  $\dot{\mathcal{P}}_E = d\mathcal{P}_E/d\tau$ . We choose  $\eta(\tau)$  to be a Gaussian switching function,  $\eta(\tau) = e^{-\tau^2/2\sigma^2}$  where  $\sigma$  is a characteristic timescale for the interaction. In the infinite interaction time limit,  $\sigma \rightarrow \infty$ , the transition rate reduces to

$$\mathcal{P}_E \propto 2\text{Re} \sum_{i,j=1}^N \int_0^\infty ds e^{-i\Omega s} \mathcal{W}^{ji}(\tau, \tau-s). \quad (19)$$

---


$$|\Psi\rangle_{FD} = \underbrace{\left[1 - \frac{\lambda^2}{N} \sum_{i=1}^N \int_{-\infty}^\infty d\tau' \chi(\tau') \int_{-\infty}^{\tau'} d\tau'' \bar{\chi}(\tau'') \hat{\Phi}(x_i(\tau')) \hat{\Phi}(x_i(\tau''))\right]}_{\mu} |0_M\rangle |g\rangle - \underbrace{\frac{i\lambda}{N} \sum_{i=1}^N \int_{-\infty}^\infty d\tau' \bar{\chi}(\tau') \hat{\Phi}(x_i(\tau'))}_{v} |0_M\rangle |e\rangle \quad (20)$$


---

where  $\mu|0_M\rangle$  and  $v|0_M\rangle$  are orthogonal field states. Given a measurement of the system at the proper time  $\tau$ , the detector is in a superposition of the ground and excited states, weighted by the amplitudes  $\mu$  and  $v$ . Importantly, these amplitudes need not be monotonic with  $\tau$ , as they contain field operators evaluated along different trajectories. In spacetime regions where the motion changes rapidly, the interplay between these terms may induce destructive interference which *decreases* the probability of excitation. In this way, the instantaneous transition rate in Eq. (19) may take on negative values, whereas Eq. (17), representing the excitation probability, is strictly positive. Since the excitation of the detector is derived from a product of first-order interactions (i.e.  $\sigma(\tau')|g\rangle$ ), we must be careful not to interpret negative transition rates as resulting from second-order processes, such as detector excitation followed by emission.

In Sec. III, we evaluate Eq. (19) numerically to obtain the instantaneous transition rate for the quantum-controlled detector. Our analysis of the conditional excitation probability – obtained for a short interaction with a Gaussian switching function – is qualitatively different to that of the instantaneous transition rate, which is analysed in the infinite interaction time limit and measured while the interaction is still on.

### III. TWO-TRAJECTORY SUPERPOSITIONS

As an application of our general, perturbative expressions, we consider a UdW detector travelling in a superposition of two uniformly accelerated trajectories, in three classes of trajectory configurations. The first two classes, parallel and anti-parallel accelerations, are studied in [10] in a two-detector entanglement harvesting scenario, and are described by the fol-

As with  $\mathcal{P}_E$ , the instantaneous transition rate  $\dot{\mathcal{P}}_E$  contains local ( $i = j$ ) and non-local ( $i \neq j$ ) terms.

It has been noted previously that Eq. (17) may represent the fraction of identically prepared detectors within a single ensemble that have undergone a transition after observation at time  $\tau$  [5, 15, 20]. Since any observation alters the state of the system, Eq. (17) no longer carries this interpretation after the measurement. Therefore, Eq. (19) compares the fraction of excited detectors in one ensemble, measured at  $\tau + \delta\tau$ , with that of another identically prepared ensemble measured at  $\tau$ , in the limit  $\delta\tau \rightarrow 0^+$ . A characteristic of Eq. (19) is that it may be negative for certain values of  $\tau$  [5, 15, 20]. To understand this, consider the final (unnormalised) detector-field state after a conditional measurement of the control in the state  $|c\rangle$ , given by

$$z_1 = \kappa^{-1} (\cosh(\kappa\tau) - 1) + \mathcal{L}/2 \quad (21)$$

$$z_2 = \pm \kappa^{-1} (\cosh(\kappa\tau) - 1) - \mathcal{L}/2 \quad (22)$$

$$t_1 = t_2 = \kappa^{-1} \sinh(\kappa\tau), \quad (23)$$

where the  $(+/-)$  sign refers to parallel (anti-parallel) trajectories and  $a$  is the proper acceleration. Specifically,  $\mathcal{L}$  defines the distance of closest approach as measured by an inertial observer along an arbitrary trajectory with constant  $z$  (space-time diagrams shown in Fig. 3 and 5) [10]. The third class of configurations is a superposition of trajectories with differing accelerations and sharing a common Rindler horizon (space-time diagrams shown in Fig. 6),

$$z_i^{\text{diff.}} = \kappa_i^{-1} \cosh(\kappa_i \tau) \quad (24)$$

$$t_i^{\text{diff.}} = \kappa_i^{-1} \sinh(\kappa_i \tau) \quad (25)$$

where  $i = 1, 2$  and the superscript diff. denotes quantities associated with the differing acceleration case. For all cases, the other spatial co-ordinates are taken to be zero. In the following, we use these three classes of trajectories to calculate the excitation probability of the detector, given by

$$\mathcal{P}_E = \frac{\lambda^2}{4} \sum_{i,j=1}^2 \int_{-\infty}^\infty d\tau' \chi(\tau') \int_{-\infty}^\infty d\tau'' \bar{\chi}(\tau'') \mathcal{W}^{ji}(\tau', \tau''). \quad (26)$$

For the excitation probability, we consider the simple case of a Gaussian switching function  $\eta(\tau) = \exp(-\tau^2/2\sigma^2)$  with  $\sigma \ll \kappa^{-1}$ , i.e. a short detector-field interaction. To evaluate the integrals in Eq. (26), we follow a similar approach to [10] by converting the complex Gaussian into a real Gaussian. The integration contour is shifted in the complex plane, which

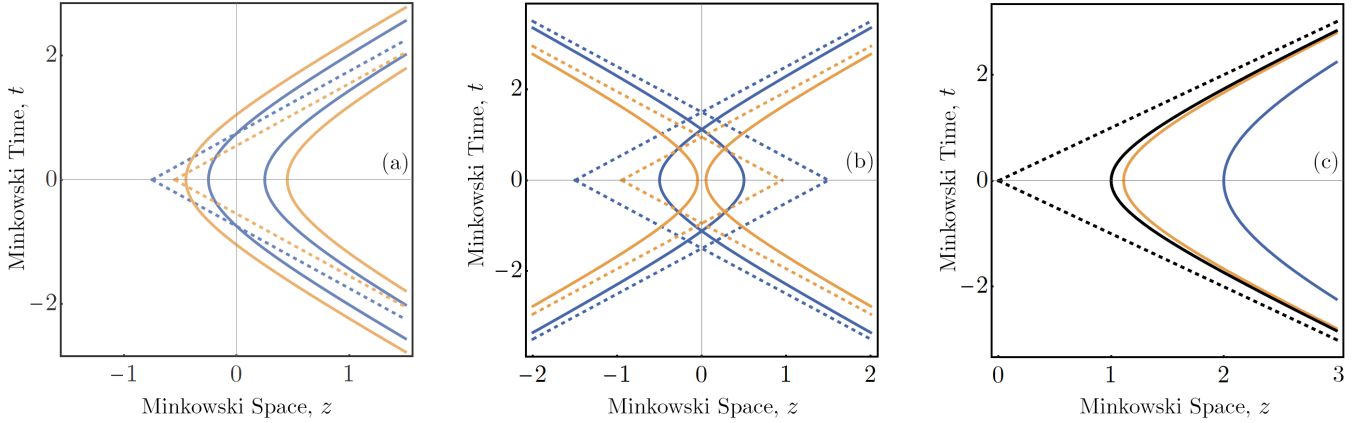


FIG. 1. Spacetime trajectories taken by the detector in a superposition of (a) parallel accelerations (with (blue)  $\mathcal{L}\kappa = 0.5$  and (orange)  $\mathcal{L}\kappa = 0.9$ ), (b) antiparallel accelerations (with (blue)  $\mathcal{L}\kappa = -1.0$  and (orange)  $\mathcal{L}\kappa = 0.1$ ) and (c) differing accelerations (with (black)  $\kappa_1 = 1.0$ , (orange)  $\kappa_2 = 0.9$  (orange) and (blue)  $\kappa_2 = 0.5$ ).

allows for evaluation using the residue theorem. Using the substitutions

$$\begin{aligned} p &= \tau' + \tau'' & \tau' &= (p + s)/2 \\ s &= \tau' - \tau'' & \tau'' &= (p - s)/2 \end{aligned} \quad (27)$$

we obtain,

$$\begin{aligned} \mathcal{P}_E &= \xi(\sigma, \Omega) \int_{-\infty}^{\infty} dp e^{-p^2/4\sigma^2} \int_{-\infty}^{\infty} ds e^{-s^2/4\sigma^2} \\ &\quad \sum_{i=1}^2 \mathcal{W}^{ii}(s - 2i\sigma^2\Omega) \\ &\quad + \xi(\sigma, \Omega) \int_{-\infty}^{\infty} dp e^{-p^2/4\sigma^2} \int_{-\infty}^{\infty} ds e^{-s^2/4\sigma^2} \\ &\quad \sum_{i \neq j}^2 \mathcal{W}^{ji}(p, s - 2i\sigma^2\Omega) + \text{res.} \end{aligned} \quad (28)$$

where the constant  $\xi(\sigma, \Omega) = (\lambda^2/8)\exp(-\sigma^2\Omega^2)$  appears after completing the square in the integrand exponent, and we have included residue terms which may appear if the contour shifted in the complex plane crosses poles. Since  $\sigma \ll \kappa^{-1}$ , the Gaussians are sharply peaked around  $p = s = 0$  for which the saddle-point approximation can be invoked [10, 11, 13]. This yields the simplified expression

$$\begin{aligned} \mathcal{P}_E &= 4\pi\sigma^2\xi(\sigma, \Omega) \left[ \sum_{i=1}^2 \mathcal{W}^{ii}(-2i\sigma^2\Omega) \right. \\ &\quad \left. + \sum_{i \neq j}^2 \mathcal{W}^{ji}(0, -2i\sigma^2\Omega) \right] + \text{res.} \end{aligned} \quad (29)$$

The single-trajectory Wightman functions used for the local terms in the transition probability and instantaneous transition rate can be easily derived using Eq. (16), given by

$$\mathcal{W}_{\text{loc.}}(s) = \frac{-1/16\pi^2}{(\kappa^{-1}\sinh(\kappa s/2) - i\varepsilon\cosh(\kappa s/2))^2}. \quad (30)$$

For future reference, the excitation probability for a single uniformly accelerated detector is given by

$$\mathcal{P}_E^{\text{loc.}} = \left( \frac{a\sigma\lambda}{2} \right)^2 \frac{e^{-\sigma^2\Omega^2}}{2\pi\sin^2(\beta)} \quad (31)$$

where  $\beta = a\sigma^2\Omega$  and the superscript (loc.) denotes the single accelerated trajectory. Notably, Eq. (31) indicates a non-thermal response – the short detector-field interaction will generally not allow the detector to reach thermal equilibrium. Our main point of comparison will be studying any deviations away from this probability when introducing a superposition of the detector's trajectory. Finally, the instantaneous transition rate for the two-trajectory superposition in the infinite interaction time limit can be expressed as

$$\begin{aligned} \dot{\mathcal{P}}_E &= \frac{1}{2} \text{Re} \sum_{i=1}^2 \int_0^{\infty} ds e^{-i\Omega s} \mathcal{W}^{ii}(s) \\ &\quad + \frac{1}{2} \text{Re} \sum_{i \neq j}^2 \int_0^{\infty} ds e^{-i\Omega s} \mathcal{W}^{ji}(\tau, \tau - s) \end{aligned} \quad (32)$$

which is a sum of the cosine and sine Fourier transforms of the Wightman functions, and can be numerically evaluated.

### A. Parallel Accelerations

Taking the positive sign in Eq. (22) for parallel accelerations, one can straightforwardly derive the Wightman functions for the interference terms,

$$\mathcal{W}_{\text{par.}}^{12}(p, s) = -\frac{1}{4\pi^2(\psi_p^2 - (\phi_p + \mathcal{L})^2)} \quad (33)$$

$$\mathcal{W}_{\text{par.}}^{21}(p, s) = -\frac{1}{4\pi^2(\psi_p^2 - (\phi_p - \mathcal{L})^2)} \quad (34)$$

where

$$\psi_p = 2\cosh(\kappa p/2)(\kappa^{-1}\sinh(\kappa s/2) - i\varepsilon\cosh(\kappa s/2)) \quad (35)$$

$$\phi_p = 2 \sinh(\kappa p/2) (\kappa^{-1} \sinh(\kappa s/2) - i\varepsilon \cosh(\kappa s/2)). \quad (36)$$

We evaluate Eq. (29) using these Wightman functions, noting

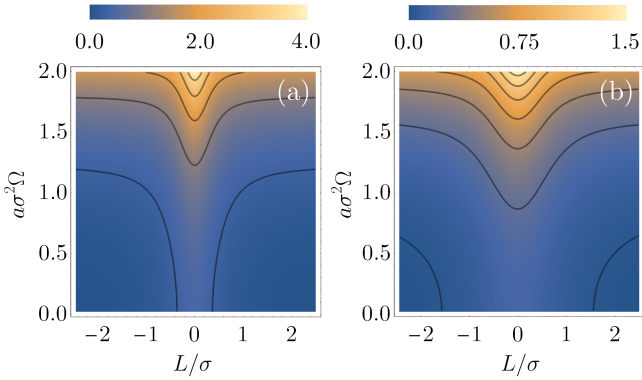


FIG. 2. Excitation probabilities,  $\mathcal{P}_E^{\text{par.}}/\lambda^2$ , for the detector in a superposition of parallel accelerations as a function of  $\mathcal{L}/\sigma$ ,  $\kappa\sigma^2\Omega$ , for (a)  $\Omega\sigma = 0.28$ , and (b)  $\Omega\sigma = 0.5$ .

that the contour shifted in the complex plane does not cross poles if we restrict our analysis to the regime  $\beta < \pi$  (see Appendix A). With this in mind, we obtain

$$\mathcal{P}_E^{\text{par.}} = \frac{\mathcal{P}_E^{\text{loc.}}}{2} + \frac{\zeta(\sigma, \Omega)}{(\kappa\mathcal{L}/2)^2 + \sin^2(\beta)} \quad (37)$$

where the superscript par. denotes parallel trajectories and  $\zeta(\sigma, \Omega) = (a\sigma\lambda)^2 e^{-\sigma^2\Omega^2}/16\pi$ . As displayed in Fig. 2, the excitation probability of the detector is maximised when the superposed paths overlap exactly. More specifically,

$$\lim_{\mathcal{L} \rightarrow 0} \mathcal{P}_E^{\text{par.}} = \mathcal{P}_E^{\text{loc.}}, \quad (38)$$

that is, the excitation probability of a single uniformly accelerated detector. In this limit, the non-local Wightman functions reduce to those for the individual trajectories; the sum of these terms, normalised by (1/4), produces Eq. (38). This is unsurprising, since for  $\mathcal{L} = 0$ , the individual worldlines fully overlap and hence there is only one accelerated trajectory. For infinitely separated trajectories, the excitation probability reduces to

$$\lim_{\mathcal{L} \rightarrow \pm\infty} \mathcal{P}_E^{\text{par.}} = \frac{\mathcal{P}_E^{\text{loc.}}}{2} \quad (39)$$

which is half of the excitation probability of a single uniformly accelerated detector. Here, the non-local Wightman functions vanish, leaving the two independent contributions from the individual accelerated trajectories. At finite separations, the field correlations between the trajectories inhibit detector excitations relative to the single-trajectory case. This result may have implications for entanglement harvesting as we note in Sec. V. Generally, the amount of entanglement that can be extracted from quantum fields onto bipartite UdW detector systems is limited by the local noise surrounding each detector. For a spatial superposition, the inhibition of excitations in the detector may provide advantages for entanglement extraction, as recent results have already suggested [35].

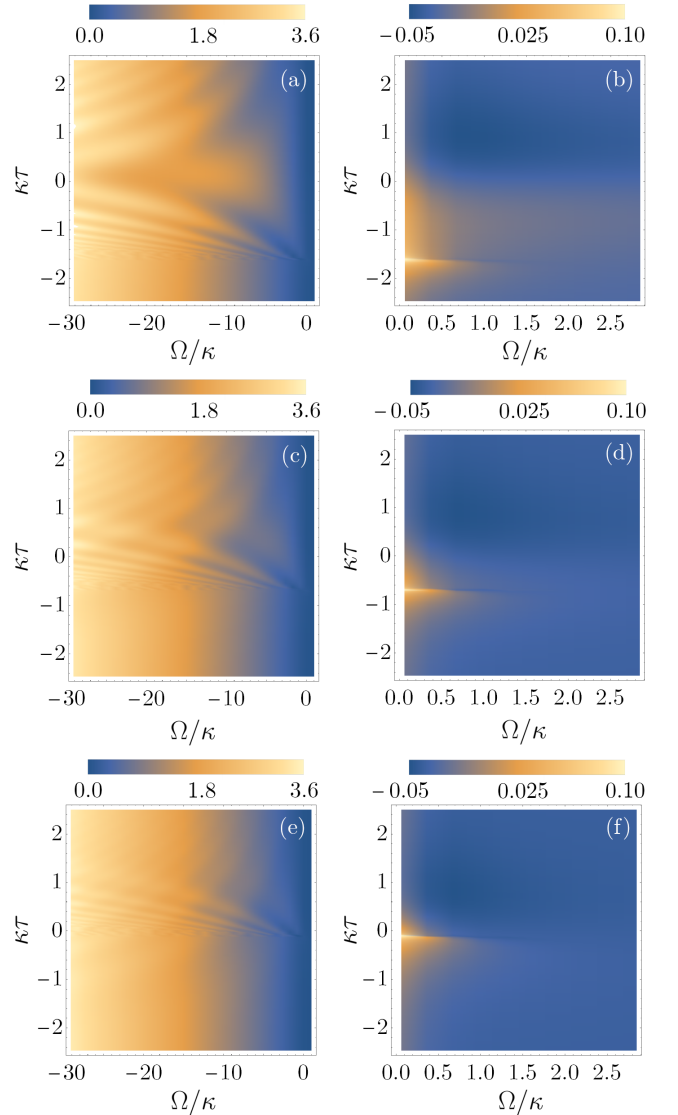


FIG. 3. Instantaneous transition rates for the detector in a superposition of parallel accelerations as a function of  $\Omega/\kappa$  and  $\kappa\tau$  for (a), (b)  $\mathcal{L}\kappa = 0.2$ , (c), (d)  $\mathcal{L}\kappa = 0.5$ , and (e), (f)  $\mathcal{L}\kappa = 0.9$ .

The instantaneous transition rate of the detector is shown in Fig. 3, for three values of  $\mathcal{L}$ . For  $\Omega < 0$ ,  $\dot{\mathcal{P}}_E$  represents the rate of stimulated emission for the detector initialised in its excited state, while  $\Omega > 0$  corresponds to the excitation rate for the detector initialised in its ground state. Notably, the energy spectrum of the detector in Fig. 3 is not just the Planckian distribution of a single uniformly accelerated detector, but exhibits time-dependent behaviour that also depends on the energy gap,  $\Omega$ . We observe how the emission (absorption) rate experiences a sudden onset of oscillations (sudden amplification or inhibition, dependent on  $\Omega$ ) at a certain proper time. These dynamics begin to manifest as the left-most trajectory ( $t_1, z_1$ ) crosses the light-like Rindler horizon of the right-most trajectory ( $t_2, z_2$ ). This rapid behaviour does not reappear as the detector recedes from the origin – that is, as the right-most trajectory passes through the lightcone of the left-most

trajectory. We conjecture that it is produced by the build-up of detector-field interactions that are transmitted through the field from the asymptotic past of the right-most trajectory. For large  $\tau$ , the non-local correlation functions become negligible and the transition rate equilibrates towards the stationary value of a single detector.

Crucially, the novel behaviour of the transition rate, most prominently observed at the horizon-crossing event, arises because the causal relationship between the trajectories is asymmetric in time. That is, the causal influence of the right-most trajectory with the left-most trajectory, mediated by the non-local field correlations between them, is not identical to that of the left-most trajectory upon the right-most trajectory. A comparable scenario without this asymmetry is a detector superposed along two inertial trajectories separated by a fixed distance  $\mathcal{L}$  and immersed in a thermal bath at the finite temperature  $T_{\text{th.}} = \kappa(2\pi)^{-1}$ . The causal relationship between the trajectories is now symmetric, and does not possess the Rindler wedge structure of the accelerated trajectories. While the response of the detector along either inertial trajectory is identical to that for the uniformly accelerated detector in the Minkowski vacuum, the non-local terms take the form [19, 36]

$$\begin{aligned} \mathcal{W}_{\text{th.}}^{12}(s) &= \mathcal{W}_{\text{th.}}^{21}(s) \\ &= \frac{\kappa(\coth \frac{\kappa}{2}(\mathcal{L} - s') + \coth \frac{\kappa}{2}(\mathcal{L} + s'))}{16\pi^2 \mathcal{L}} \end{aligned} \quad (40)$$

where  $s' = \tau - \tau' - i\epsilon$ . Notably,  $\mathcal{W}_{\text{th.}}^{12} = \mathcal{W}_{\text{th.}}^{21}$  are time-translation invariant (depending only on  $s = \tau' - \tau''$ ), implying that the transition rate of such a detector is *time-independent*. This demonstrates that the physical trajectories of the detector non-trivially affect its response by changing the detector's proper time, along with the causal relations and ordering of the interactions along the individual paths. By using compactly supported switching functions which confine the interactions to localised spacetime regions, our approach motivates further studies of the detector interacting with the field regions in quantum-controlled causal orders [25, 26].

## B. Anti-Parallel Accelerations

As a direct comparison to the parallel scenario, we now study the detector travelling in a superposition of accelerated paths in anti-parallel motion. Taking the minus sign in Eq. (21)-(23), we derive the non-local correlation functions between the trajectories,

$$\begin{aligned} \mathcal{W}_{\text{anti.}}^{12}(p, s) &= \mathcal{W}_{\text{anti.}}^{21}(p, s) \\ &= -\frac{1}{4\pi^2(\psi_a^2 - (\phi_a - 2\kappa^{-1} + \mathcal{L})^2)} \end{aligned} \quad (41)$$

and

$$\psi_a = 2\cosh(\kappa p/2)(\kappa^{-1} \sinh(\kappa s/2) - i\epsilon \cosh(\kappa s/2)) \quad (42)$$

$$\phi_a = 2\cosh(\kappa p/2)(\kappa^{-1} \cosh(\kappa s/2) - i\epsilon \sinh(\kappa s/2)). \quad (43)$$

Using Eq. (28) and confirming that no poles are crossed while

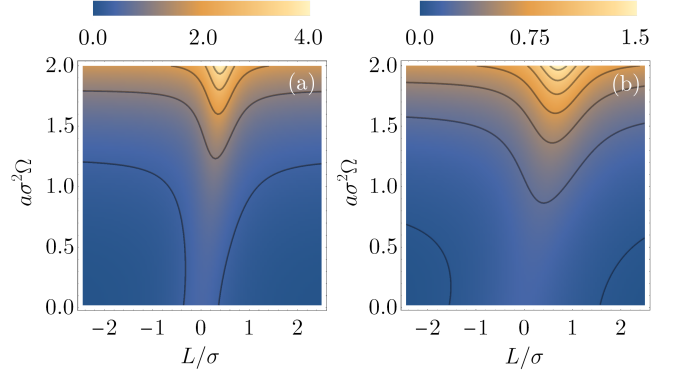


FIG. 4. Excitation probabilities,  $\mathcal{P}_E^{\text{anti.}}/\lambda^2$ , for the detector in a superposition of antiparallel accelerations as a function of  $\mathcal{L}/\sigma$ ,  $\kappa\sigma^2\Omega$ , for (a)  $\Omega\sigma = 0.28$ , and (b)  $\Omega\sigma = 0.5$ .

shifting the contour of integration, we find that

$$\mathcal{P}_E^{\text{anti.}} = \frac{\mathcal{P}_E^{\text{loc.}}}{2} + \frac{\zeta(\sigma, \Omega)}{\sin^2(\beta) + (\cos(\beta) + (\kappa\mathcal{L}/2 - 1))^2}. \quad (44)$$

As shown in Fig. 4, the conditional excitation probability is asymmetric with respect to  $\mathcal{L} = 0$ , reflecting the asymmetry of the configurations for the  $\mathcal{L} < 0$  and  $\mathcal{L} > 0$  cases. This quantitative difference with the parallel case demonstrates that interference effects between the trajectories depend explicitly on their physical configuration, along with the respective space-time regions that they traverse. Furthermore, it can be straightforwardly shown that for  $\beta = \kappa\sigma^2\Omega \ll 1$ ,  $\mathcal{P}_E^{\text{anti.}}$  approaches  $\mathcal{P}_E^{\text{par.}}$ , where we emphasise that this response is characteristically non-thermal. In such a regime, the trajectories are approximately inertial and hence, the distinction between parallel and anti-parallel motion is nullified.

Analogous to the parallel acceleration case, the excitation probability at infinite separation is half of the excitation probability for a single uniformly accelerated detector,

$$\lim_{\mathcal{L} \rightarrow \pm\infty} \mathcal{P}_E^{\text{anti.}} = \frac{\mathcal{P}_E^{\text{loc.}}}{2}. \quad (45)$$

The factor of (1/2) can be traced back to the vanishing of the non-local Wightman functions and the normalisation of the initial state of the control superposition. When  $\mathcal{L} = 0$ , the conditional excitation probability is

$$\lim_{\mathcal{L} \rightarrow 0} \mathcal{P}_E^{\text{anti.}} = \frac{\mathcal{P}_E^{\text{loc.}}}{2} + \frac{\zeta(\sigma, \Omega)}{2(1 - \cos(\beta))} \quad (46)$$

which differs from the parallel acceleration scenario, in the same limit. This demonstrates that the physical configuration of the trajectories has a significant role in determining the detector's response. Comparing Eq. (37) and (44), it is clear that the non-local field correlations between the trajectories produce different interference effects which non-trivially inhibit excitations.

The instantaneous transition rate of the detector is shown in Fig. 5, for three values of  $\mathcal{L}$ . When  $\mathcal{L} \leq 0$ , the intersection

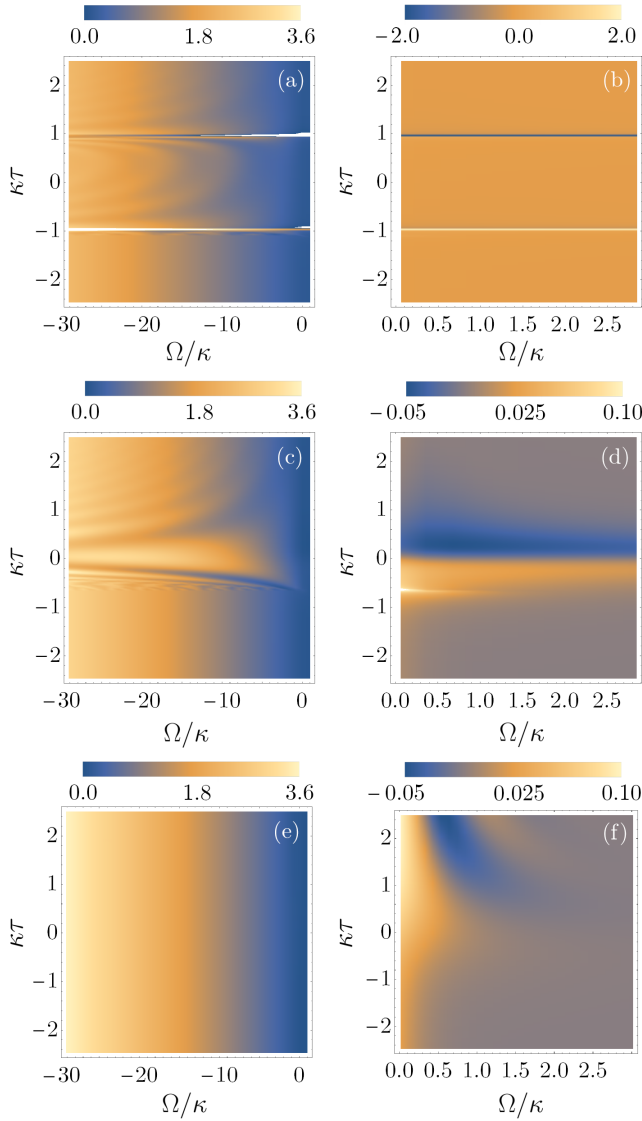


FIG. 5. Instantaneous transition rates for the detector in a superposition of antiparallel accelerations as a function of  $\Omega/\kappa$  and  $\kappa\tau$  for (a), (b)  $\mathcal{L}\kappa = -1.0$ , (c), (d)  $\mathcal{L}\kappa = 0.1$ , and (e), (f)  $\mathcal{L}\kappa = 2.0$ .

of the Rindler wedges forms a diamond within which the trajectories are causally connected. Inside this diamond region, the emissive and absorptive response of the detector changes rapidly at two proper times, a phenomenon related to the crossings of the trajectories. When  $0 < \mathcal{L} < 2\kappa^{-1}$ , the trajectories are not spacelike separated, but do not overlap spatially. In a comparable manner to the parallel motion, the transition rate is approximately time-independent until the detector-field interactions from the asymptotic past become causally connected with the spacetime region of the other trajectory, at which the emission (absorption) rate becomes highly oscillatory (is suddenly inhibited). For  $\mathcal{L} > 2\kappa^{-1}$ , the trajectories are spacelike separated and the effect of the non-local terms in  $\dot{\mathcal{P}}_E$  decreases with  $\mathcal{L}$ . In this scenario, the Rindler horizon of either trajectory never intersects the other, suppressing the dramatic dynamical effects observed at the horizon-crossing

event for the causally connected trajectories.

### C. Detector Thermalisation

It is interesting to consider if the detector ever exhibits an exactly thermal response, as is the case for a single trajectory. The transition rate must satisfy the detailed balance form of the Kubo-Martin-Schwinger (KMS) condition [37],

$$\frac{\dot{\mathcal{P}}_E(\Omega)}{\dot{\mathcal{P}}_E(-\Omega)} = \exp(-2\pi\Omega/\kappa). \quad (47)$$

Recalling that  $\mathcal{L}$  defines the distance of closest approach between the two trajectories, we find that for both the parallel and anti-parallel configurations, the KMS condition is only satisfied in the limit  $\mathcal{L} \rightarrow \pm\infty$ . In this regime, the field correlations between the individual trajectories is zero, characterised by the vanishing of the non-local Wightman functions in Eq. (32). The transition rate reduces to

$$\lim_{\mathcal{L} \rightarrow \pm\infty} \dot{\mathcal{P}}_E^{\text{anti.}} = \lim_{\mathcal{L} \rightarrow \pm\infty} \dot{\mathcal{P}}_E^{\text{par.}} = \text{Re} \int_0^\infty ds e^{-i\Omega s} \mathcal{W}_{\text{loc.}}(s). \quad (48)$$

Using Eq. (30) for the single-trajectory Wightman function, evaluating the contour integral as per [4] and letting  $\varepsilon \rightarrow 0$  after the integration yields

$$\lim_{\mathcal{L} \rightarrow \pm\infty} \dot{\mathcal{P}}_E^{\text{anti.}} = \lim_{\mathcal{L} \rightarrow \pm\infty} \dot{\mathcal{P}}_E^{\text{par.}} = \frac{\Omega}{4\pi} \frac{1}{\exp(2\pi\Omega/a) - 1}, \quad (49)$$

which is half of the transition rate for a single, uniformly accelerated detector – satisfying Eq. (47) – in agreement with the results found for the excitation probability. Importantly, for finitely separated trajectories in the superposition, the presence of non-zero, time-dependent field correlations between them always alters the detector’s response from being exactly thermal. Infinitely separated trajectories possessing different proper accelerations do not produce a thermal response either.

### D. Differing Accelerations

Finally, we consider the detector travelling in a superposition of uniformly accelerated paths with differing proper accelerations  $\kappa_1$  and  $\kappa_2$ , using the co-ordinates defined in Eq. (24) and (25). The non-local Wightman functions are

$$\mathcal{W}_{\text{diff.}}^{12}(\tau', \tau'') = -\frac{1}{4\pi^2(\psi_{12}^2 - \phi_{12}^2)} \quad (50)$$

$$\mathcal{W}_{\text{diff.}}^{21}(\tau', \tau'') = -\frac{1}{4\pi^2(\psi_{21}^2 - \phi_{21}^2)} \quad (51)$$

where

$$\psi_{ij} = \varsigma_{ij} - 2i\varepsilon \cosh(\alpha_{-}^{ij}) \cosh(\alpha_{+}^{ij}) \quad (52)$$

$$\phi_{ij} = \chi_{ij} - 2i\varepsilon \cosh(\alpha_{-}^{ij}) \sinh(\alpha_{+}^{ij}) \quad (53)$$

with

$$\varsigma_{ij} = \kappa_i^{-1} \sinh(\kappa_i \tau') - \kappa_j^{-1} \sinh(\kappa_j \tau'') \quad (54)$$

$$\chi_{ij} = \kappa_i^{-1} \cosh(\kappa_i \tau') - \kappa_j^{-1} \cosh(\kappa_j \tau'') \quad (55)$$

and  $\alpha_{\pm}^{ij} = (\kappa_i \tau' \pm \kappa_j \tau'')/2$ . For  $\kappa_1 = \kappa_2$ , Eq. (50) and (51) reduce to the Wightman function for a single accelerated trajectory. Unlike the parallel and anti-parallel cases, shifting the contours of integration crosses poles in the Wightman functions. Nevertheless, the usual procedure can still be applied

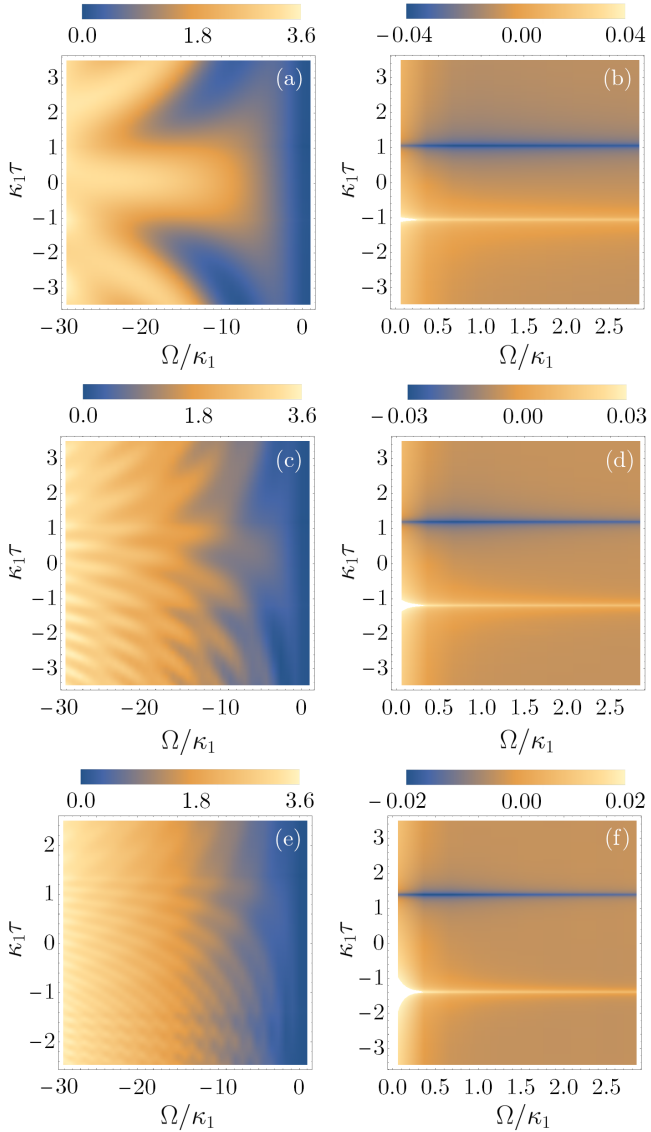


FIG. 6. Instantaneous transition rates for the detector in a superposition of differing accelerations as a function of  $\Omega/\kappa$  and  $\kappa\tau$  for (a), (b)  $\kappa_2/\kappa_1 = 0.5$ , (c), (d)  $\kappa_2/\kappa_1 = 0.7$ , and (e), (f)  $\kappa_2/\kappa_1 = 0.9$ .

to obtain a semi-analytic result with the inclusion of residue contributions,

$$\begin{aligned} \mathcal{P}_E^{\text{diff.}} = & \left( \frac{\sigma\lambda}{2} \right)^2 \frac{e^{-\sigma^2\Omega^2}}{8\pi} \left[ \frac{\kappa_1^2}{\sin^2(\beta_1)} + \frac{\kappa_2^2}{\sin^2(\beta_2)} \right. \\ & \left. + \frac{8\kappa_1^2\kappa_2^2}{\kappa_1^2 + \kappa_2^2 - 2\kappa_1\kappa_2 \cos(\beta_1 + \beta_2)} \right] + \text{res.} \quad (56) \end{aligned}$$

where  $\beta_i = \kappa_i \sigma^2 \Omega$ . Since the residue contributions are difficult to obtain analytically, we leave a quantitative analysis of the excitation probability for future work. Nevertheless, by inspecting Eq. (56), we discover independent contributions to  $\mathcal{P}_E^{\text{diff.}}$  from the individual trajectories, as well as an interference term between them. Furthermore, it is possible to analyse two simple cases. The first occurs in the limit when  $\kappa_1 = \kappa_2$  whereby the residue contributions vanish, yielding the excitation probability for a single accelerated detector,

$$\lim_{\kappa_1 \rightarrow \kappa_2} \mathcal{P}_E^{\text{diff.}} = \lim_{\mathcal{L} \rightarrow 0} \mathcal{P}_E^{\text{par.}} = \mathcal{P}_E^{\text{loc.}}. \quad (57)$$

The other occurs when one acceleration approaches zero, for which the excitation probability is given by

$$\lim_{\kappa_1 \rightarrow 0} \mathcal{P}_E^{\text{diff.}} = \frac{\mathcal{P}_E^{\text{loc.}}(\kappa_2)}{4} + \left( \frac{\lambda}{2\sigma\Omega} \right)^2 \frac{e^{-\sigma^2\Omega^2}}{8\pi} + \text{res.} \quad (58)$$

In this form, the transition probability contains a constant contribution from the inertial trajectory, while the contribution from the acceleration is one-quarter of that for a single accelerated detector. That the detector registers a non-zero particle count along the inertial trajectory can be understood as a consequence of the energy-time uncertainty relation,  $\Delta t \Delta E \geq 1$ . Since the detector-field interaction is localised in time, the contribution from the inertial trajectory is non-zero even when the field is in the vacuum state [14].

For the instantaneous transition rate,  $\tau$  represents the equal proper time along the respective trajectories at which the detector is measured, recalling Eq. (17). Because the trajectories possess differing proper accelerations, and subsequently, differing proper times, the transition rate cannot be defined with respect to a global time coordinate in the inertial reference frame. As shown in Fig. 6, the emission rate exhibits sustained oscillations since the distance between the paths of the superposition changes constantly according to an inertial observer. The frequency of these oscillations is blue-shifted (red-shifted) as the detector approaches (recedes from) the origin, indicating that the dynamics are affected by causal relationships between the trajectories, similar to those observed previously.

For the absorption rate, we observe three qualitatively distinct regions of behaviour: the detector approaching the origin,  $\tau \lesssim -1$  (increasing absorption of field quanta, approaching a point of rapid amplification), the turning point of the trajectories,  $-1 \lesssim \tau \lesssim 1$  (a decreasing rate, transitioning to negative values), and recession from the origin,  $\tau \gtrsim 1$  (period of rapid decrease in the absorption rate, reaching a minimal turning point, before equilibration to zero). We associate the cusp-like points of the transition rate with spacetime regions where the quantum-controlled motion of the detector induces rapid changes in the field states, recalling Eq. (20). As noted, the negative values can be understood in light of the multiple detector ensemble interpretation of the transition rate.

#### IV. COHERENCE OF THE SUPERPOSITION

We previously considered the specific case where the control degree of freedom was measured in its initial state,  $|c\rangle$ .

However in general, the final state of the control need not necessarily equal its initial superposition. For example, the detector-field interaction may cause the individual control states  $|c_i\rangle$  associated with the respective trajectories to evolve by some relative phase. Consider the general case wherein the control is measured in the final state

$$|c\rangle_F = \frac{1}{\sqrt{N}} \sum_{i=1}^N e^{-i\varphi_i} |c_i\rangle. \quad (59)$$

The final state of the detector is described by the following density matrix,

$$\hat{\rho}_D = \frac{1}{N^2} \sum_{i,j=1}^N e^{-i(\varphi_i - \varphi_j)} \hat{\rho}_{ij,D}, \quad (60)$$

where the individual contributions  $\rho_{ij,D}$  take the form of Eq. (11). Performing the sum over  $i, j$  yields the following (un-normalised) result, derived in Appendix B

$$\begin{aligned} \hat{\rho}_D = \frac{1}{N^2} & \left[ |g\rangle\langle g| \left\{ N + 2 \sum_{i=1}^N \sum_{\substack{j=2 \\ j>i}}^N \cos(\varphi_i - \varphi_j) - 2\lambda^2 \sum_{i=1}^N \iint_{\mathcal{T}} \mathcal{W}^{ii} - 2\lambda^2 \sum_{i=1}^N \sum_{\substack{j=2 \\ i < j}}^N \cos(\varphi_i - \varphi_j) \iint_{\mathcal{T}} (\mathcal{W}^{ii} + \mathcal{W}^{jj}) \right\} \right. \\ & \left. + \lambda^2 |e\rangle\langle e| \left\{ \sum_{i=1}^N \iint \mathcal{W}^{ii} + \sum_{i=1}^N \sum_{\substack{j=2 \\ j>i}}^N \left[ e^{-i(\varphi_i - \varphi_j)} \iint \mathcal{W}^{ji} + e^{-i(\varphi_j - \varphi_i)} \iint \mathcal{W}^{ij} \right] \right\} \right] \end{aligned} \quad (61)$$

where we have adopted the integral notation

$$\iint_{\mathcal{T}} = \int_{-\infty}^{\infty} d\tau' \chi(\tau') \int_{-\infty}^{\tau'} d\tau'' \bar{\chi}(\tau'') \quad (62)$$

$$\iint = \int_{-\infty}^{\infty} d\tau' \chi(\tau') \int_{-\infty}^{\infty} d\tau'' \bar{\chi}(\tau''). \quad (63)$$

For illustration, let us examine the  $N = 2$  case, where the elements of the density matrix are

$$\begin{aligned} 1 - \mathcal{P}_G^{N=2} &= \frac{1}{2} \left[ \left\{ 1 - \lambda^2 \iint_{\mathcal{T}} (\mathcal{W}^{11} + \mathcal{W}^{22}) \right\} \right. \\ &\quad \left. \times (1 + \cos(\varphi_1 - \varphi_2)) \right] \end{aligned} \quad (64)$$

$$\begin{aligned} \mathcal{P}_E^{N=2} &= \frac{\lambda^2}{4} \left[ \iint (\mathcal{W}_+^{11} + \mathcal{W}_+^{22}) + e^{-i(\varphi_1 - \varphi_2)} \iint \mathcal{W}^{21} \right. \\ &\quad \left. + e^{-i(\varphi_2 - \varphi_1)} \iint \mathcal{W}^{12} \right] \end{aligned} \quad (65)$$

Recall that the sum of Eq. (64) and (65) gives the normalisation of the final state of the detector, conditioned upon the control being measured in the superposition state, Eq. (59). Equivalently, this is the probability amplitude for the detector-field state conditioned upon the final state of the control:

$$\langle \Psi | \Psi \rangle_{FD}^{N=2} = 1 - \mathcal{P}_G^{N=2} + \mathcal{P}_E^{N=2} \quad (66)$$

We notice that  $\langle \Psi | \Psi \rangle_{FD}^{N=2}$  depends on the relative phase  $\Delta\varphi = \varphi_1 - \varphi_2$ . In interferometric terms, this suggests that the control state retains some coherence after the interaction, which is quantified by the so-called visibility – generally, the amplitude of oscillation as the relative phase  $\varphi_1 - \varphi_2$  is varied. In particular, by varying the relative phase, the probability in Eq. (66) oscillates around  $(1/2)$  with a small amplitude, suppressed in the weak coupling limit (i.e.  $\lambda \ll 1$ ). This implies that the

evolution of the system, mediated by the interaction, causes the control to become (weakly, on the order of  $\lambda^2$ ) entangled with the detector-field system.

### A. A Note on the Control

In Sec. II A, we introduced the control degree of freedom  $c_i$  which initialises the superposition, without specific reference to a physical model. Several proposals for the physical implementation of UdW detector superpositions have been studied in the literature. For example, [38] considers how a measurement of the Berry phase acquired by an accelerating detector may allow for a measurement of the Unruh effect at significantly lower accelerations than ordinarily required. In that paper, the authors propose an in-principle atomic interferometry setup [39] which causes the detector to travel in a superposition of an inertial and accelerated path. In [40, 41], the authors consider another in-principle setup where single UdW detectors are sent through a beamsplitter which allows them to extract unknown information localised to cavities along the respective arms. [41] uses this to model a quantum thermometer, allowing the detector to measure the temperature of a cold reservoir relative to a hotter reservoir, without requiring that the detector reach thermal equilibrium. These works provide feasible schemes wherein our quantum-controlled detector model could be physically realised.

Finally, we note that a detection of the interference effects presented in this paper would be on the same order of difficulty as a measurement of the Unruh effect itself. It is well-known that accelerations of  $\sim 10^{20} \text{ m/s}^2$  are required to register an Unruh temperature of  $1 \text{ K}$  – hence, we expect that accelerations to this order or larger would be required to observe perturbations away from the expected detector response.

## V. CONCLUSION

In this paper, we have established a general framework for a UdW detector travelling in a quantum superposition of classical trajectories, by introducing an additional degree of freedom which could create and control such a superposition. To second-order in perturbation theory, we derived the final state of a detector traversing an arbitrary superposition of paths, and subsequently its conditional excitation probability and instantaneous transition rate. This final state, including the instantaneous transition rate, depends on *local* two-point correlation functions evaluated along each individual trajectory, as well as *non-local* or *interference* terms between the trajectories. For particular scenarios involving two-trajectory superpositions of accelerated paths in parallel and anti-parallel motion, we derived semi-analytic expressions for the excitation probability of the detector.

Notably, we discovered that even for a superposition of paths with the same proper acceleration (parallel and anti-parallel trajectories), the final state of the detector differs from that of a single trajectory, and in particular is not thermal. In contrast, if the detector followed either of the individual trajectories, it would register the same thermal response. A thermal response is recovered for infinite separation between the trajectories in the superposition. Our numerical results for the instantaneous transition rate revealed novel interference effects not observed in the single detector scenario. In the parallel and anti-parallel scenarios, we discovered sudden periods of rapid, oscillatory behaviour in the transition rate, which revealed a dependence on causal dynamics between the trajectories. For the detector travelling in a superposition of proper accelerations, these causal relations induced Doppler-shifting of the oscillations in the emission rate as the detector approached, then receded from the origin.

Our new approach can be directly applied to scenarios of fundamental interest in quantum field theory, cosmology and even quantum gravity. For example, it can be used to describe an UdW detector in a spacetime produced by a black hole in quantum superposition of different masses, or a detector in superposition of falling into a black hole and escaping it. Via the equivalence principle, we can also simulate spacetimes with entangled temporal order [26] by considering Rindler observers with entangled proper accelerations [27]. Other tra-

jectories and spacetimes of interest, such as the de Sitter and anti-de Sitter geometries can also be studied by exploiting the well-known relationships between these spacetimes, Rindler geometry and conformal field theory [10, 19].

From a broader perspective, our results suggest a connection between recent works studying coherent control of quantum channels [28–31, 42], relativistic quantum information [32], and quantum thermodynamics [33]. Here, the interaction between an UdW detector and a quantum field, facilitated by the coherent control of the detectors’ trajectory, directly results in a quantum control of different channels acting on the detector. It has been shown [30, 31, 42] that quantum control can result in increased channel capacities. Quantum-controlled UdW detectors can thus be exploited from the perspective of reducing the unavoidable noise experienced by non-inertial parties (due to the Unruh effect) in any relativistic quantum information setting. This expectation is further corroborated by recent findings in [35] showing that quantum control of the interaction time of inertial UdW detectors with a quantum field allows the detectors to become entangled in scenarios where this is otherwise impossible [43].

Secondly, from the perspective of quantum thermodynamics, the quantum-controlled UdW model introduces a new scenario, a quantum control of thermalisation channels. Quantum aspects of temperature are of high interest and relevance to this field [44] and our approach paves the way for answering foundational questions about the physical meaning and phenomenology associated with coherent control of temperatures. Already, the present results hint at a rich structure of the problem, as we have found that the quantum control of channels yielding the same Unruh temperature, in general do not result in any thermalisation of the system.

Note added: towards the completion of this work we became aware of an independent study on a similar topic by Barbado, Castro-Ruiz, Apadula and Brukner, see [arXiv:2003.12603](https://arxiv.org/abs/2003.12603).

## VI. ACKNOWLEDGEMENTS

The authors would like to thank Robert Mann for fruitful discussions. We acknowledge support from the Australian Research Council Centre of Excellence for Quantum Computation and Communication Technology (Project No. CE170100012) and DECRA Grant DE180101443.

## Appendix A: Complex Integration

### 1. Parallel Accelerations

Firstly, recall that the non-local correlation functions for the parallel acceleration case take the form:

$$\mathcal{W}_{\text{par.}}^{12}(p, s) = -\frac{1}{4\pi^2(\psi_p^2 - (\phi_p + \mathcal{L})^2)} \quad (\text{A1})$$

$$\mathcal{W}_{\text{par.}}^{21}(p, s) = -\frac{1}{4\pi^2(\psi_p^2 - (\phi_p - \mathcal{L})^2)} \quad (\text{A2})$$

where

$$\psi_p = 2 \cosh(\kappa p/2) (\kappa^{-1} \sinh(\kappa s/2) - i\epsilon \cosh(\kappa s/2)) \quad (\text{A3})$$

$$\phi_p = 2 \sinh(\kappa p/2) (\kappa^{-1} \sinh(\kappa s/2) - i\epsilon \cosh(\kappa s/2)). \quad (\text{A4})$$

We must account for residue contributions to the integral whenever  $\mathcal{W}_{\text{par.}}^{12}$  or  $\mathcal{W}_{\text{par.}}^{21}$  diverge for complex  $s$ . Without loss of generality, we can absorb  $\cosh(\kappa s/2)$  into  $\epsilon$  which yields the following condition for a divergence in  $\mathcal{W}_{\text{par.}}^{ij}$ ,

$$0 = (2\kappa^{-1} \sinh(\kappa s/2) \cosh(\kappa p/2) - i\epsilon)^2 - (2\kappa^{-1} \sinh(\kappa s/2) \sinh(\kappa p/2) - i\epsilon \pm \mathcal{L})^2. \quad (\text{A5})$$

Expanding the brackets, absorbing further terms into  $\epsilon$  and then re-arranging, yields the following equation

$$\sinh(\kappa p/2) = \pm \left( (\kappa \mathcal{L})^{-1} \sinh(\kappa s/2) - \frac{a\mathcal{L}}{4} \operatorname{csch}(\kappa s/2) + i\epsilon \right). \quad (\text{A6})$$

Since we are shifting the  $s$ -integrand in the complex plane, we may express  $s = s_r + is_i$  as a sum of real and imaginary parts. Applying this substitution and then taking the imaginary part of the equation yields the following constraint equation,

$$0 = \sin(\kappa s_i/2) \cosh(\kappa s_r/2) \left[ (\kappa \mathcal{L})^{-1} - \frac{\kappa \mathcal{L}}{2} \frac{1}{\cos(\kappa s_r) - \cosh(\kappa s_i)} \right] + \epsilon. \quad (\text{A7})$$

Firstly, notice that poles occur whenever  $\sin(\kappa s_i/2) = 0$ , that is, when  $\kappa s_i/2 = \pi n + \epsilon$ . Since the contour is shifted by  $2\sigma^2 \Omega$  in the complex plane, we obtain the constraint

$$2\sigma^2 \Omega < \frac{2\pi}{\kappa} \quad (\text{A8})$$

$$\beta < \pi \quad (\text{A9})$$

as stated in the body of the paper. Furthermore, the bracketed term is never zero – since we invoke the saddle-point approximation at  $s_r = 0$ , this requires

$$\frac{(\kappa \mathcal{L})^2}{2} = 1 - \cosh(\kappa s_i) \quad (\text{A10})$$

which is only satisfied for  $a = 0$ , a case we do not explicitly consider. We also need to consider the real part of the pole constraint equation. Expanding Eq. (A5) and absorbing terms into  $\epsilon$  without loss of generality, yields

$$0 = 4\kappa^{-2} \sinh^2(\kappa s/2) \mp 4\kappa^{-1} \mathcal{L} \sinh(\kappa p/2) \sinh(\kappa s/2) - \mathcal{L}^2 \pm i\epsilon. \quad (\text{A11})$$

Expressing  $s = s_r + is_i$  and taking the real part of the equation leaves

$$0 = \sinh^2(\kappa s_r/2) \cos^2(\kappa s_i/2) - \cosh^2(\kappa s_r/2) \sin^2(\kappa s_i/2) \mp \kappa \mathcal{L} \sinh(\kappa p/2) \sinh(\kappa s_r/2) \cos(\kappa s_i/2) - \left( \frac{\kappa \mathcal{L}}{2} \right)^2. \quad (\text{A12})$$

The saddle-point approximation assumes  $s_r = 0$ , which leaves

$$0 = \sin^2(\kappa s_i/2) + \left( \frac{\kappa \mathcal{L}}{2} \right)^2 \quad (\text{A13})$$

which is never satisfied. Hence, the only relevant constraint is Eq. (A9).

## 2. Anti-Parallel Accelerations

The non-local correlation functions for the anti-parallel acceleration case are given by

$$\mathcal{W}_{\text{anti.}}^{12}(p, s) = \mathcal{W}_{\text{anti.}}^{21}(p, s) = -\frac{1}{4\pi^2(\psi_a^2 - (\phi_a - 2\kappa^{-1} + \mathcal{L})^2)} \quad (\text{A14})$$

where

$$\psi_a = 2 \cosh(\kappa p/2) (\kappa^{-1} \sinh(\kappa s/2) - i\epsilon \cosh(\kappa s/2)) \quad (\text{A15})$$

$$\phi_a = 2 \cosh(\kappa p/2) (\kappa^{-1} \cosh(\kappa s/2) - i\epsilon \sinh(\kappa s/2)). \quad (\text{A16})$$

Again, absorbing terms into  $\epsilon$  without loss of generality yields the following constraint,

$$0 = [2\kappa^{-1} \sinh(\kappa s/2) \cosh(\kappa p/2) - i\epsilon]^2 - [2\kappa^{-1} \sinh(\kappa s/2) \sinh(\kappa p/2) - i\epsilon - 2\kappa^{-1} + \mathcal{L}]^2. \quad (\text{A17})$$

Expanding the brackets and absorbing terms into  $\epsilon$  leaves

$$0 = 4\kappa^{-2} \sinh^2(\kappa s/2) + \sinh(\kappa s/2) \sinh(\kappa p/2) (8\kappa^{-1} - 4\kappa^{-1} \mathcal{L}) - (\mathcal{L} + 2\kappa^{-1})^2 + i\epsilon. \quad (\text{A18})$$

Re-arranging this equation and making the association  $s = s_r + is_i$  yields,

$$\sinh(\kappa p/2) = \frac{\sinh(\kappa(s_r + is_i)/2)}{2(\kappa\mathcal{L}/2 - 1)} + \frac{4(\kappa\mathcal{L}/2 + 1)^2}{\kappa^2 \operatorname{csch}(\kappa(s_r + is_i)/2)} + i\epsilon. \quad (\text{A19})$$

The imaginary part of Eq. (A19) is

$$0 = \sin(\kappa s_i/2) \cosh(\kappa s_r/2) \left[ \frac{(\kappa\mathcal{L}/2 - 1)^{-1}}{2} + \frac{8}{\kappa^2} \frac{(\kappa\mathcal{L}/2 + 1)^2}{\cos(\kappa s_i) - \cosh(\kappa s_r)} \right] + \epsilon \quad (\text{A20})$$

which gives the same constraint as the parallel acceleration case,  $\beta < \pi$ . For the bracketed term with  $s_r = 0$ , we find that

$$\frac{\kappa^2}{16} \frac{1}{(\kappa\mathcal{L}/2 - 1)(\kappa\mathcal{L}/2 + 1)^2} = \frac{1}{1 - \cos(\kappa s_i)} \quad (\text{A21})$$

The right-hand side is strictly positive (recalling that we consider the cases where  $s_i < 2\sigma^2\Omega$ ), while the left-hand side negative for  $a\mathcal{L}/2 < 1$ , before diverging and crossing a pole near  $a\mathcal{L}/2 = 1$ . We thus restrict our analysis to the regime where the the pole condition is not satisfied. As with the parallel acceleration case, we also consider the real part of the constraint equation. Performing the substitution  $s = s_r + is_i$  and taking the real part of Eq. (A18) yields

$$0 = \sinh^2(\kappa s_r/2) \cos^2(\kappa s_i/2) - \cosh^2(\kappa s_r/2) \sin^2(\kappa s_i/2) + 2(\kappa - \mathcal{L}) \sinh(\kappa p/2) \sinh(\kappa s_r/2) \cos(\kappa s_i/2) - (\kappa\mathcal{L}/2 + 1)^2. \quad (\text{A22})$$

At  $s_r = 0$ , we have the constraint equation for the pole, given by  $\sin^2(\kappa s_i/2) = -(\kappa\mathcal{L}/2 + 1)^2$ , which is never satisfied. Hence, our analysis does not require the evaluation of residue contributions so long as  $\beta < \pi$ .

## Appendix B: Measuring the Control in an Arbitrary Superposition

Here, we derive the final state of the detector given that the control is measured in some arbitrary superposition state. Using the integral notation of Eq. (62) and (63), we can express Eq. (60) in full

$$\begin{aligned} \hat{\rho}_D = & \frac{1}{N^2} \left[ |g\rangle\langle g| + \lambda^2 |e\rangle\langle e| \iint \mathcal{W}^{11} - 2\lambda^2 |g\rangle\langle g| \iint_{\mathcal{T}} \mathcal{W}^{11} + \dots + |g\rangle\langle g| + \lambda^2 |e\rangle\langle e| \iint \mathcal{W}^{NN} - 2\lambda^2 |g\rangle\langle g| \iint_{\mathcal{T}} \mathcal{W}^{NN} \right. \\ & + e^{-i(\varphi_1 - \varphi_2)} \left\{ |g\rangle\langle g| + \lambda^2 |e\rangle\langle e| \iint \mathcal{W}^{21} - \lambda^2 |g\rangle\langle g| \iint_{\mathcal{T}} (\mathcal{W}^{11} + \mathcal{W}^{22}) \right\} + (1 \leftrightarrow 2) \\ & + \dots + e^{-i(\varphi_1 - \varphi_N)} \left\{ |g\rangle\langle g| + \lambda^2 |e\rangle\langle e| \iint \mathcal{W}^{N1} - \lambda^2 |g\rangle\langle g| \iint_{\mathcal{T}} (\mathcal{W}^{11} + \mathcal{W}^{NN}) \right\} + (1 \leftrightarrow N) + \dots \\ & \left. + \dots + e^{-i(\varphi_{N-1} - \varphi_N)} \left\{ |g\rangle\langle g| + \lambda^2 |e\rangle\langle e| \iint \mathcal{W}^{N(N-1)} - \lambda^2 |g\rangle\langle g| \iint_{\mathcal{T}} (\mathcal{W}^{(N-1)(N-1)} + \mathcal{W}^{NN}) \right\} + (N-1 \leftrightarrow N) \right]. \quad (\text{B1}) \end{aligned}$$

Collecting terms together and simplifying yields

$$\hat{\rho}_D = \frac{1}{N^2} \left[ N |g\rangle\langle g| + \lambda^2 |e\rangle\langle e| \sum_{i=1}^N \iint \mathcal{W}^{ii} - 2\lambda^2 |g\rangle\langle g| \sum_{i=1}^N \iint_{\mathcal{T}} \mathcal{W}^{ii} \right]$$

$$\begin{aligned}
& + 2|g\rangle\langle g| \cos(\varphi_1 - \varphi_2) - 2\lambda^2|g\rangle\langle g| \cos(\varphi_1 - \varphi_2) \iint_{\mathcal{T}} (\mathcal{W}^{11} + \mathcal{W}^{22}) \\
& + \dots + 2|g\rangle\langle g| \cos(\varphi_1 - \varphi_N) - 2\lambda^2|g\rangle\langle g| \cos(\varphi_1 - \varphi_N) \iint_{\mathcal{T}} (\mathcal{W}^{11} + \mathcal{W}^{NN}) \\
& + \dots + 2|g\rangle\langle g| \cos(\varphi_{N-1} - \varphi_N) - 2\lambda^2|g\rangle\langle g| \cos(\varphi_{N-1} - \varphi_N) \iint_{\mathcal{T}} (\mathcal{W}^{(N-1)(N-1)} + \mathcal{W}^{NN}) \\
& + \lambda^2|e\rangle\langle e| \left\{ e^{-i(\varphi_1 - \varphi_2)} \iint \mathcal{W}^{21} + e^{-i(\varphi_2 - \varphi_1)} \iint \mathcal{W}^{12} \right\} \\
& + \dots + \lambda^2|e\rangle\langle e| \left\{ e^{-i(\varphi_1 - \varphi_N)} \iint \mathcal{W}^{N1} + e^{-i(\varphi_N - \varphi_1)} \iint \mathcal{W}^{1N} \right\} \\
& + \dots + \lambda^2|e\rangle\langle e| \left\{ e^{-i(\varphi_{N-1} - \varphi_N)} \iint \mathcal{W}^{N(N-1)} + e^{-i(\varphi_N - \varphi_{N-1})} \iint \mathcal{W}^{(N-1)N} \right\} \quad (B2)
\end{aligned}$$

This is the expanded form of Eq. (60).

---

[1] W. G. Unruh and R. M. Wald, *Phys. Rev. D* **29**, 1047 (1984).

[2] W. G. Unruh, *Phys. Rev. D* **14**, 870 (1976).

[3] P. C. W. Davies and A. C. Ottewill, *Phys. Rev. D* **65**, 104014 (2002).

[4] S. Schlicht, *Classical and Quantum Gravity* **21**, 4647 (2004).

[5] J. Louko and A. Satz, *Classical and Quantum Gravity* **23**, 6321 (2006).

[6] S.-Y. Lin and B. L. Hu, *Phys. Rev. D* **76**, 064008 (2007).

[7] E. G. Brown, E. Martín-Martínez, N. C. Menicucci, and R. B. Mann, *Phys. Rev. D* **87**, 084062 (2013).

[8] D. E. Bruschi, A. R. Lee, and I. Fuentes, *Journal of Physics A: Mathematical and Theoretical* **46**, 165303 (2013).

[9] D. C. Ostapchuk, S.-Y. Lin, R. B. Mann, and B. Hu, *JHEP* **07**, 072 (2012), arXiv:1108.3377 [gr-qc].

[10] G. Salton, R. B. Mann, and N. C. Menicucci, *New Journal of Physics* **17**, 035001 (2015).

[11] S. Kukita and Y. Nambu, *Classical and Quantum Gravity* **34**, 235010 (2017).

[12] E. Martín-Martínez and N. C. Menicucci, *Classical and Quantum Gravity* **31**, 214001 (2014).

[13] Y. Nambu, *Entropy* **15**, 1847 (2013), arXiv:1305.4193 [gr-qc].

[14] G. V. Steeg and N. C. Menicucci, *Phys. Rev. D* **79**, 044027 (2009).

[15] J. Louko and A. Satz, *Classical and Quantum Gravity* **25**, 055012 (2008).

[16] L. Hodgkinson and J. Louko, *Phys. Rev. D* **86**, 064031 (2012), arXiv:1206.2055 [gr-qc].

[17] L. Hodgkinson, J. Louko, and A. C. Ottewill, *Phys. Rev. D* **89**, 104002 (2014), arXiv:1401.2667 [gr-qc].

[18] K. K. Ng, L. Hodgkinson, J. Louko, R. B. Mann, and E. Martín-Martínez, *Phys. Rev. D* **90**, 064003 (2014), arXiv:1406.2688 [quant-ph].

[19] N. D. Birrell and P. Davies, *Quantum fields in curved space*, 7 (Cambridge university press, 1984).

[20] P. Langlois, *Annals Phys.* **321**, 2027 (2006), arXiv:gr-qc/0510049.

[21] L. Hodgkinson and J. Louko, *Journal of Mathematical Physics* **53**, 082301 (2012), <https://doi.org/10.1063/1.4739453>.

[22] B. L. Hu, S.-Y. Lin, and J. Louko, *Classical and Quantum Gravity* **29**, 224005 (2012).

[23] N. Stritzelberger and A. Kempf, *Phys. Rev. D* **101**, 036007 (2020).

[24] F. Giacomini, E. Castro-Ruiz, and v. C. Brukner, *Nature Communications* **10** (2019), 10.1038/s41467-018-08155-0.

[25] O. Oreshkov, F. Costa, and v. C. Brukner, *Nature Communications* **3** (2012), 10.1038/ncomms2076.

[26] M. Zych, F. Costa, I. Pikovski, and v. C. Brukner, *Nature Commun.* **10**, 3772 (2019), arXiv:1708.00248 [quant-ph].

[27] A. Dimić, M. Milivojević, D. Gočanin, and Časlav Brukner, “Simulating spacetime with indefinite causal order *via* rindler observers,” (2017), arXiv:1712.02689 [quant-ph].

[28] D. K. L. Oi, *Phys. Rev. Lett.* **91**, 067902 (2003).

[29] D. Ebler, S. Salek, and G. Chiribella, *Phys. Rev. Lett.* **120**, 120502 (2018).

[30] G. Chiribella and H. Kristjánsson, *Proceedings of the Royal Society A: Mathematical, Physical and Engineering Sciences* **475**, 20180903 (2019).

[31] A. A. Abbott, J. Wechs, D. Horsman, M. Mhalla, and C. Branciard, “Communication through coherent control of quantum channels,” (2018), arXiv:1810.09826 [quant-ph].

[32] R. B. Mann and T. C. Ralph, *Classical and Quantum Gravity* **29**, 220301 (2012).

[33] S. Vinjanampathy and J. Anders, *Contemporary Physics* **57**, 545 (2016).

[34] A. Satz, *Classical and Quantum Gravity* **24**, 1719 (2007).

[35] L. J. Henderson, A. Belenchia, E. Castro-Ruiz, C. Budroni, M. Zych, Časlav Brukner, and R. B. Mann, “Quantum temporal superposition: the case of qft,” (2020), arXiv:2002.06208 [quant-ph].

[36] H. A. Weldon, *Physical Review D* **62** (2000), 10.1103/physrevd.62.056010.

[37] R. Haag, N. M. Hugenholtz, and M. Winnink, *Communications in Mathematical Physics* **5**, 215 (1967).

[38] E. Martín-Martínez, I. Fuentes, and R. B. Mann, *Physical Review Letters* **107** (2011), 10.1103/physrevlett.107.131301.

[39] K. Bongs, M. Holynski, J. Vovrosh, P. Bouyer, G. Condon, E. Rasel, C. Schubert, W. P. Schleich, and A. Roura, *Nature Reviews Physics*, 1 (2019).

[40] M. Onuma-Kalu, R. B. Mann, and E. Martín-Martínez, *Physical Review A* **88** (2013), 10.1103/physreva.88.063824.

- [41] E. Martín-Martínez, A. Dragan, R. B. Mann, and I. Fuentes, *New Journal of Physics* **15**, 053036 (2013).
- [42] P. A. Guérin, G. Rubino, and i. c. v. Brukner, *Phys. Rev. A* **99**, 062317 (2019).
- [43] P. Simidzija, R. H. Jonsson, and E. Martín-Martínez, *Phys. Rev. D* **97**, 125002 (2018).
- [44] H. J. D. Miller and J. Anders, *Nature Communications* **9** (2018), 10.1038/s41467-018-04536-7.